molecules

MDPI

Article

Chloro- and Dichloro-methylsulfonyl Nitrenes: Spectroscopic Characterization, Photoisomerization, and Thermal Decomposition

Yang Yang [1], Xianxu Chu [1], Yan Lu [1], Manabu Abe [2,*] and Xiaoqing Zeng [1,*]

[1] College of Chemistry, Chemical Engineering and Materials Science, Soochow University, Suzhou 215123, China; 20174209103@stu.suda.edu.cn (Y.Y.); 20164209104@stu.suda.edu.cn (X.C.); 20164209106@stu.suda.edu.cn (Y.L.)

[2] Department of Chemistry, Graduate School of Science, Hiroshima University, 1-3-1 Kagamiyama, Higashi-Hiroshima, Hiroshima 739-8526, Japan

* Correspondence: xqzeng@suda.edu.cn (X.Z.); mabe@hiroshima-u.ac.jp (M.A.); Tel.: +86-51265880090 (X.Z.); +81-824247432 (M.A.)

Academic Editor: Xuefeng Wang
Received: 27 November 2018; Accepted: 12 December 2018; Published: 13 December 2018

Abstract: Chloro- and dichloro-methylsulfonyl nitrenes, $CH_2ClS(O)_2N$ and $CHCl_2S(O)_2N$, have been generated from UV laser photolysis (193 and 266 nm) of the corresponding sulfonyl azides $CH_2ClS(O)_2N_3$ and $CHCl_2S(O)_2N_3$, respectively. Both nitrenes have been characterized with matrix-isolation IR and EPR spectroscopy in solid N_2 (10 K) and glassy toluene (5 K) matrices. Triplet ground-state multiplicity of $CH_2ClS(O)_2N$ ($|D/hc|$ = 1.57 cm^{-1} and $|E/hc|$ = 0.0026 cm^{-1}) and $CHCl_2S(O)_2N$ ($|D/hc|$ = 1.56 cm^{-1} and $|E/hc|$ = 0.0042 cm^{-1}) has been confirmed. In addition, dichloromethylnitrene $CHCl_2N$ ($|D/hc|$ = 1.57 cm^{-1} and $|E/hc|$ = 0 cm^{-1}), formed from SO_2-elimination in $CHCl_2S(O)_2N$, has also been identified for the first time. Upon UV light irradiation (365 nm), the two sulfonyl nitrenes R–$S(O)_2N$ (R = CH_2Cl and $CHCl_2$) undergo concomitant 1,2-R shift to *N*-sulfonylamines R–NSO_2 and 1,2-oxygen shift to *S*-nitroso compounds R–S(O)NO, respectively. The identification of these new species with IR spectroscopy is supported by ^{15}N labeling experiments and quantum chemical calculations at the B3LYP/6-311++G(3df,3pd) level. In contrast, the thermally-generated sulfonyl nitrenes $CH_2ClS(O)_2N$ (600 K) and $CHCl_2S(O)_2N$ (700 K) dissociate completely in the gas phase, and in both cases, HCN, SO_2, HCl, HNSO, and CO form. Additionally, ClCN, $OCCl_2$, $HNSO_2$, $\bullet NSO_2$, and the atmospherically relevant radical $\bullet CHCl_2$ are also identified among the fragmentation products of $CHCl_2S(O)_2N$. The underlying mechanisms for the rearrangement and decomposition of $CH_2ClS(O)_2N$ and $CHCl_2S(O)_2N$ are discussed based on the experimentally-observed products and the calculated potential energy profile.

Keywords: azides; nitrenes; decomposition; matrix isolation; photoisomerization; reaction mechanism

1. Introduction

Nitrenes R–N are neutral species containing monovalent nitrogen atoms [1]. Chemically, nitrenes are highly reactive intermediates that have been extensively used in chemical transformations such as the well-known aziridination and C–H amidation reactions, and also in the covalent functionalization of nanomaterials [2–4]. Typically, nitrenes R–N can be readily generated from the decomposition of azides R–N_3 upon either photolysis or pyrolysis, in which molecular nitrogen is the only byproduct [5]. However, due to inherent instability and also high reactivity of nitrenes, the associated rapid intramolecular rearrangement and/or intermolecular reactions with solvent molecules in solution render their direct observations challenging. Therefore, conventional chemical trapping reactions have

been frequently used to probe the structure and reactivity of nitrenes [6,7]. The direct characterization of nitrenes requires either ultrafast [8–10] or cryogenic matrix-isolation spectroscopic methods [11–13]. Recently, relatively more stable nitrenes stabilized by bulky organic ligands have also been synthesized as isolable compounds even at room temperatures [14].

Compared to the intensively studied alkyl [15], aryl [16,17], and carbonyl nitrenes [18–20], knowledge about the fundamental properties of sulfonyl nitrenes $RS(O)_2$–N is limited, although this class of nitrenes have been frequently proposed as the key intermediate in the synthesis of *N*-sulfonyl-1,2,3-triazoles [21], biologically relevant sulfonamides [22], and diamines [23], where sulfonyl azides $RS(O)_2$–N_3 were usually used as the reagents. As the most frequently studied targets, naphthyl [8,10], phenyl [9], and methyl-substituted [9] sulfonyl nitrenes have already been directly observed in the photolytic decomposition of the corresponding azide precursors in solution by using ultrafast IR spectroscopy, and triplet ground-state multiplicity has been also established with EPR spectroscopy. Interestingly, experimental studies by chemical trapping [24] and ultrafast kinetics [8–10] in solutions have revealed that sulfonyl nitrenes are generally more rigid than carbonyl nitrenes RC(O)–N, since the latter may undergo facile rearrangement to isocyanate RNCO through 1,2-R shift [18]. In contrast, similar 1,2-R shift in sulfonyl nitrenes to *N*-sulfonlyamines R–NSO_2, known as pseudo-Curtius rearrangement, has been only occasionally observed in the photochemistry of sulfonyl azides under matrix-isolation conditions [11,25,26]. Moreover, *S*-nitroso compounds R–S(O)NO, formally regarded as the 1,2-oxygen shifted isomers of sulfonyl nitrenes R–$S(O)_2N$, have been identified among the photolysis products of fluorinated sulfonyl nitrenes such as $CF_3S(O)_2$–N [12] and $FS(O)_2$–N [13].

In addition to the complex photochemistry of sulfonyl nitrenes in solution and cryogenic matrices, their thermal decompositions were found to yield diverse fragments, thus providing access to some highly reactive species in the gas phase. For instance, the thermolysis of $FS(O)_2$–N [11] yields sulfonyl radical FSO_2• and N_2 via nitrene dimerization. Fragmentation of $CH_3S(O)_2$–N and $CF_3S(O)_2$–N [27] furnishes iminyl radical •NSO_2 through homolytic C–S bond cleavage. Flash vacuum pyrolysis of $CH_3OS(O)_2$–N [26] and $PhS(O)_2$–N [28] forms $HNSO_2$ and Ph–N with concerted elimination of CH_2O and SO_2, respectively.

The distinct photolytic and thermal chemistry of various sulfonyl nitrenes prompted us to extend our studies to other sulfonyl nitrenes, including the barely investigated chlorinated methylsulfonyl nitrenes $CH_nX_{3-n}ClS(O)_2N$ (n = 0–2), the key intermediates in the decomposition of the synthetically useful chloromethylsulfonyl azides [29]. Herein, we report the first generation and spectroscopic characterization of triplet sulfonyl nitrenes $CH_2ClS(O)_2N$ and $CHCl_2S(O)_2N$ in cryogenic matrices. In addition to the photolytic rearrangement products *N*-sulfonlyamines R–NSO_2 and *S*-nitroso compounds R–S(O)NO, a novel triplet chloromethylnitrene species $CHCl_2N$ has also been identified. Furthermore, the complex decomposition of the two nitrenes in the gas phase has been presented. Unlike the dominant C–S bond cleavage in $CH_3S(O)_2$–N [27], thermal decompositions of $CH_2ClS(O)_2N$ and $CHCl_2S(O)_2N$ initiate mainly by the concomitant elimination of HCl and SO_2.

2. Results and Discussion

2.1. Photolysis of $CH_2ClS(O)_2N_3$

The photolysis of $CH_2ClS(O)_2N_3$ in solid N_2-matrix was performed by using an ArF excimer laser (193 nm). The IR difference absorption spectrum reflecting the decomposition of the azide is shown in Figure 1A. Upon irradiation, nearly 42% of the azide was depleted. As a result, new species with IR bands at 1354.1, 1155.5, and 500.8 cm^{-1} formed. These band positions are close to those of SO_2 (1347.5, 1153.1, and 524.6 cm^{-1}) [30]. In addition, several weak but distinguishable IR bands in the range of 900–700 cm^{-1} appear but partially overlap with those of the azide precursor.

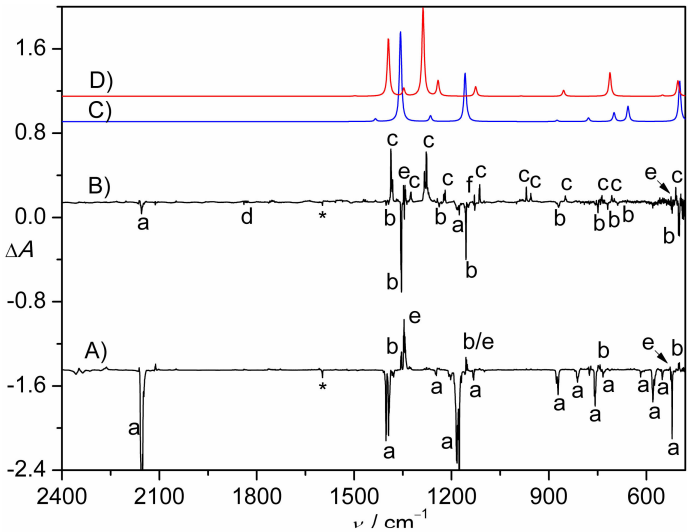

Figure 1. (**A**) IR difference spectrum (Absorbance, Δ*A*) showing the decomposition of $CH_2ClS(O)_2N_3$ in N_2-matrix upon a 193 nm laser photolysis (30 min); (**B**) IR difference spectrum (Absorbance, Δ*A*) showing the change of the N_2-matrix upon subsequent UV-light photolysis (365 nm, 8 min). For clarity, spectrum B is 12-fold expanded along the Δ*A* axis. (**C**) Calculated IR spectrum of triplet $CH_2ClS(O)_2N$ at the B3LYP/6-311++G(3df,3pd) level. (**D**) Calculated IR spectrum of CH_2ClNSO_2 at the B3LYP/6-311++G(3df,3pd) level. The IR bands of $CH_2ClS(O)_2N_3$ (a), $CH_2ClS(O)_2N$ (b), CH_2ClNSO_2 (c), $CH_2ClS(O)NO$ (d), SO_2 (e), unknown species (f), and impurity H_2O (*) are labeled. For clarity, the spectra are arbitrarily shifted along the Δ*A* axis.

Given the TD-B3LYP/6-311++G(3df,3pd) calculated vertical transition at 390 nm (oscillator strength f = 0.0084, Table S1) for the most likely candidate species $CH_2ClS(O)_2N$, the matrix containing the 193 nm laser photolysis products of $CH_2ClS(O)_2N_3$ was further irradiated with UV-light (365 nm). The resulting IR difference absorption spectrum (Figure 1B) suggests the depletion of trace azide but mainly the carrier for the aforementioned new IR bands (1354.1, 1155.5, and 500.8 cm^{-1}). The selective depletion enables the unambiguous identification of the remaining weak IR bands for this carrier at 3023.0, 2953.6, 1398.3, 1238.6, 1128.2, 870.1, 748.8, 718.9, and 688.1 cm^{-1} (Table 1). Most of these band positions agree with the calculated IR frequencies for the expected nitrene intermediate $CH_2ClS(O)_2N$ in the triplet state (Figure 1C).

Table 1. Calculated and observed IR frequencies (>500 cm^{-1}) of $CH_2ClS(O)_2N$.

Calculated [a]				Observed [b]		Assignment [c]
Singlet		Triplet		N_2-matrix		
ν	Δν	ν	Δν	ν	Δν	
3183 (4)	0.0	3176 (2)	0.0	3023.0 (4)	<0.5	$\nu_{asym}(CH_2)$
3098 (5)	0.0	3097 (3)	0.0	2953.6 (7)	<0.5	$\nu_{sym}(CH_2)$
1431 (5)	0.0	1435 (4)	0.0	1398.3 (3)	<0.5	$\delta(CH_2)$
1400 (164)	2.5	1357 (155)	0.0	1354.1 (100)	<0.5	$\nu_{asym}(SO_2)$
1268 (13)	0.1	1265 (10)	0.0	1238.6 (6)	<0.5	$\omega(CH_2)$
1161 (1)	0.0	1158 (83)	0.0	1155.5 (40)	<0.5	$\nu_{sym}(SO_2)$
1053 (67)	9.4	1149 (2)	0.0	1128.2 (5)	<0.5	$\tau(CH_2)$
973 (12)	11.5	875 (2)	0.0	870.1 (8)	<0.5	$\varrho(CH_2)$
870 (<1)	0.1	778 (6)	0.3	748.8 (9)	<0.5	ν(CCl)
761 (21)	0.5	699 (15)	11.2	718.9 (6)	11.1	ν(SN)
686 (16)	0.9	656 (26)	0.2	688.1 (7)	<0.5	ν(SC)
515 (83)	3.0	497 (69)	4.0	500.8 (42)	<0.5	$\delta(SO_2)$

[a] The calculated IR harmonic frequencies (ν, unscaled), ^{15}N-isotopic shifts (Δν), and band intensities (km mol^{-1}, in parentheses) for the singlet and triplet states at the B3LYP/6-311++G(3df,3pd) level. Full list of the calculated IR frequencies for all the conformers are given in Table S2. [b] The observed band positions (ν), ^{15}N-isotopic shifts (Δν), and relative intensities (in parentheses) in N_2-matrix. [c] Tentative assignment based on the calculated vibrational displacement vectors for the triplet state.

According to the calculated vibrational displacement vectors of triplet $CH_2ClS(O)_2N$, the two characteristic stretching vibrations of the SO_2 moiety are located at 1354.1 ($\nu_{asym}(SO_2)$) and 1155.5 cm^{-1} ($\nu_{sym}(SO_2)$), which are very close to those of other triplet sulfonyl nitrenes such as $CH_3S(O)_2N$ (1349.8 and 1156.6 cm^{-1}, Ne-matrix) [31], $CF_3S(O)_2N$ (1387.4 and 1171.8 cm^{-1}, Ar-matrix) [12], and $PhS(O)_2N$ (1348.9 and 1168.2 cm^{-1}, Ne-matrix) [28]. No noticeable shift occurs to both IR bands in the ^{15}N-labeled nitrene. Only one band at 718.9 cm^{-1} displays a large ^{15}N isotopic shift of 11.1 cm^{-1}, which is in good agreement with the calculated shift of 11.2 cm^{-1} for the S–N stretching mode (Table 1). It is also close to those in $CH_3S(O)_2N$ (11.0 cm^{-1}) [31] and $CF_3S(O)_2N$ (8.2 cm^{-1}) [12]. It should be noted that the calculated S–N stretching mode in singlet $CH_2ClS(O)_2N$ locates at 973 cm^{-1} ($\Delta\nu_{cal}(^{14/15}N)$ = 11.5 cm^{-1}). Moreover, the two SO_2 stretching vibrations in the nitrene in the singlet state at 1400 and 1053 cm^{-1} are heavily mixed with the S–N stretching mode, as evidenced by the calculated ^{15}N isotopic shifts of 2.5 and 9.4 cm^{-1}, respectively. The absence of these bands in the IR spectrum of the photolysis products of $CH_2ClS(O)_2N_3$ (Figure 1) suggests that the initially-generated singlet nitrene $CH_2ClS(O)_2N$ from the N_2-elimination in the azide relaxes to the triplet ground state through rapid intersystem crossing (ISC). According to the recent ultrafast spectroscopic studies on the kinetics of arylsulfonyl nitrenes in solutions, the ISC from singlet to triplet is extremely fast (700 ± 300 ps in CCl_4) [8,10].

As can be seen in Figure 1B, the UV-light irradiation (365 nm) results in the depletion of the nitrene $CH_2ClS(O)_2N$ and another species with a weak IR band at 1839.6 cm^{-1} (labeled with d in Figure 1B). It exhibits a large ^{15}N-isotopic shift of 32.1 cm^{-1}. Both the band position and isotopic shift are very close to those of the most prominent N=O stretching vibration in $CF_3S(O)NO$ (ν(NO) = 1832.3 cm^{-1}, $\Delta\nu(^{14/15}N)$ = 32.0 cm^{-1}, Ar-matrix) [12]. Furthermore, they also show good agreement with the calculated strongest IR band for the oxygen-shifted rearrangement product $CH_2ClS(O)NO$ (ν_{cal}(NO) = 1838 cm^{-1}, $\Delta\nu_{cal}(^{14/15}N)$ = 32.1 cm^{-1}, Table S3). Nevertheless, the observation of only one band renders the identification of $CH_2ClS(O)NO$ tentative. In contrast, the formation of the 1,2-CH_2Cl shifted rearrangement product CH_2ClNSO_2 from the 365 nm irradiation of nitrene $CH_2ClS(O)_2N$ can be assured by the occurrence of one set of IR bands at 1470.3, 1387.0, 1324.7, 1278.0, 1219.7, 1113.1, 967.7, 849.4, 706.4, and 509.3 cm^{-1}. Interestingly, each of these bands is accompanied with a weaker matrix-site band (Table 2), probably due to interactions of CH_2ClNSO_2 with the surrounding molecules in the matrix cages. The assignment is supported by the good agreement of the observed frequencies and ^{15}N-isotopic shifts with the calculations (Figure 1D).

Table 2. Calculated and observed IR frequencies (>500 cm^{-1}) of CH_2ClNSO_2.

Calculated [a]		Observed (N_2-matrix) [b]		Assignment [c]
ν	Δν	ν	Δν	
3166 (<1)	0.0			ν_{asym} (CH_2)
3096 (8)	0.0			ν_{sym} (CH_2)
1497 (1)	0.3	1470.3/1465.3 (2)	<0.5	δ (CH_2)
1394 (198)	0.3	1387.0/1381.6 (57)	<0.5	ν_{asym} (SO_2)
1347 (26)	4.2	1326.0/1324.7 (10)	4.4	ω (CH_2) + ν (N=S)
1287 (303)	11.6	1283.7/1278.0 (100)	10.4	ν (N=S)
1241 (52)	0.8	1224.2/1219.7 (14)	<0.5	τ (CH_2)
1125 (33)	15.5	1114.6/1113.1 (13)	15.5	ν (CN) + ν_{sym} (SO_2)
985 (1)	2.6	967.7/955.9 (12)	<0.5	ϱ (CH_2)
854 (20)	9.1	849.4/846.7 (7)	8.8	ν (C–N–S)
712 (81)	0.8	706.4/699.0 (11)	2.3	ν (CCl)
550 (4)	6.0			δ (S–O–N)
502 (53)	2.0	509.3/506.7 (8)	2.2	δ (SO_2)

[a] The calculated IR harmonic frequencies (ν, unscaled), ^{15}N-isotopic shifts (Δν), and intensities (km mol^{-1}, in parentheses) at the B3LYP/6-311++G(3df,3pd) level. Full list of the calculated IR frequencies for all the conformers are given in Table S4. [b] The observed band positions (ν), ^{15}N-isotopic shifts (Δν), and relative band intensities (in parentheses) in N_2-matrix. [c] Tentative assignment based on the calculated vibrational displacement vectors.

In CH_2ClNSO_2, the asymmetric and symmetric SO_2 stretching vibration modes occur at 1387.0 and 1113.1 cm^{-1}, respectively, and the latter strongly couples with the C–N stretching (ν(CN)), as indicated by the ^{15}N-isotopic shift of 15.5 cm^{-1}. The ν(N=S) stretching mode appears at 1278.0 cm^{-1} ($\Delta\nu(^{14}/^{15}N)$ = 10.4 cm^{-1}). It is slightly lower than that in CH_3NSO_2 (1294.9 cm^{-1}, Ar-matrix), which has been very recently generated in the gas phase through flash vacuum pyrolysis of sulfamoyl chloride $MeN(H)S(O)_2Cl$ through HCl-elimination [32]. In addition to CH_2ClNSO_2, traces of SO_2 were also produced. However, the counterpart fragmentation species CH_2ClN or its isomer CHCl=NH was not observed due to weak IR intensities.

2.2. Flash Vacuum Pyrolysis of $CH_2ClS(O)_2N_3$

Similar to the photochemistry, the thermal decomposition of sulfonyl azides (e.g., $FS(O)_2N_3$ [11] and $PhS(O)_2N_3$ [28]) should also initiate by extruding molecular nitrogen, followed by secondary fragmentation of the sulfonyl nitrene intermediates. To uncover the thermal behavior of $CH_2ClS(O)_2N$, flash vacuum pyrolysis (FVP, 600 K) of $CH_2ClS(O)_2N_3$ in N_2 dilution (1:1000) was performed. The IR spectrum of the pyrolysis products (Figure 2A) reveals complete dissociation of the azide, fragments SO_2 (e) [33,34], HCN (g, 3287.8 and 735.5 cm^{-1}) [35], HCl (h, 2854.5, 2803.8 cm^{-1}) [32], HNSO (i, 3305.0, 1253.5, 1094.9, 925.6, and 775.5 cm^{-1}) [36], H_2CO (j, 1740.0 and 1499.7 cm^{-1}) [26], CH_2NH (k, 1637.4, 1450.9, and 1064.7 cm^{-1}) [35], HNCO (l, 3489.2 and 2265.7 cm^{-1}) [37], CO_2 (m, 2348.9 and 662.3 cm^{-1}) [38], CO (n, 2138.9 cm^{-1}) [38], and N_2 (IR inactive) form.

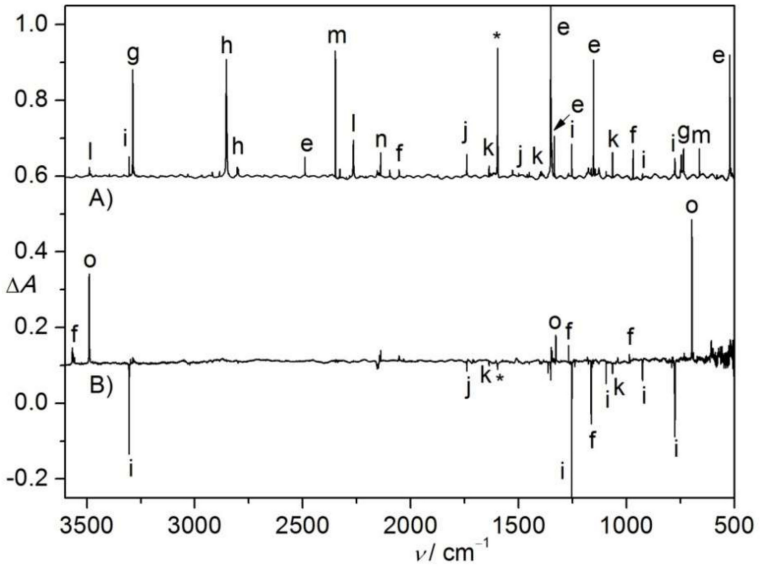

Figure 2. (**A**) IR spectrum (Absorbance, *A*) of the N_2-matrix isolated flash vacuum pyrolysis (600 K) products of $CH_2ClS(O)_2N_3$. (**B**) IR difference spectrum (Absorbance, Δ*A*) showing the change of the N_2-matrix upon subsequent 266 nm laser photolysis (25 min). For clarity, spectrum B is 12-fold expanded along the Δ*A* axis. The IR bands of SO_2 (e), unknown species (f), HCN (g), HCl (h), HNSO (i), H_2CO (j), CH_2NH (k), HNCO (l), CO_2 (m), CO (n), HOSN (o), and impurity H_2O (*) are labeled. For clarity, the spectra are arbitrarily shifted along the Δ*A* axis.

The absence of the IR band for nitrene $CH_2ClS(O)_2N$ implies its immediate dissociation under the FVP conditions. Unlike the straightforward C–S bond cleavage in other alkylsulfonyl nitrenes $CH_3S(O)_2N$ (→•CH_3 + •NSO_2) and $CF_3S(O)_2N$ (→•CF_3 + •NSO_2), the absence of the IR bands for •CH_2Cl and •NSO_2 in the IR spectrum (Figure 2A), and the presence of very strong IR bands for SO_2, mean that no C–S bond cleavage, but rather, SO_2-elimination occurs for $CH_2ClS(O)_2N$. The identification of HCl and HCN strongly suggests that further fragmentation happens to the SO_2-elimination product CH_2ClN. The unexpected formation of a second pair of fragments HNSO/HCl/CO from $CH_2ClS(O)_2N$ can be tentatively explained by first rearrangement to CH_2ClNSO,

as followed by further HCl-elimination via the intermediacy of a putative carbene species H–C–NSO_2. As further proof of the identification of HNSO among the products, the previously-observed [36,39] isomerization to HOSN was repeated by irradiation with a 266 nm laser (Figure 2B).

2.3. Photolysis of $CHCl_2S(O)_2N_3$

The photolysis of $CHCl_2S(O)_2N_3$ in N_2-matrix was also performed with a 193 nm laser. Compared to the photochemistry of $CH_2ClS(O)_2N_3$, the depletion of $CHCl_2S(O)_2N_3$ is more relatively efficient, since 52% of the azide vanishes in 11 min. In the corresponding IR difference absorption spectrum (Figure 3A), the IR bands of SO_2 (1344.4, 1150.2, and 522.4 cm^{-1}) and new species at 1835.1, 1777.3, 1366.5, 1153.2, and 512.6 cm^{-1} can be identified.

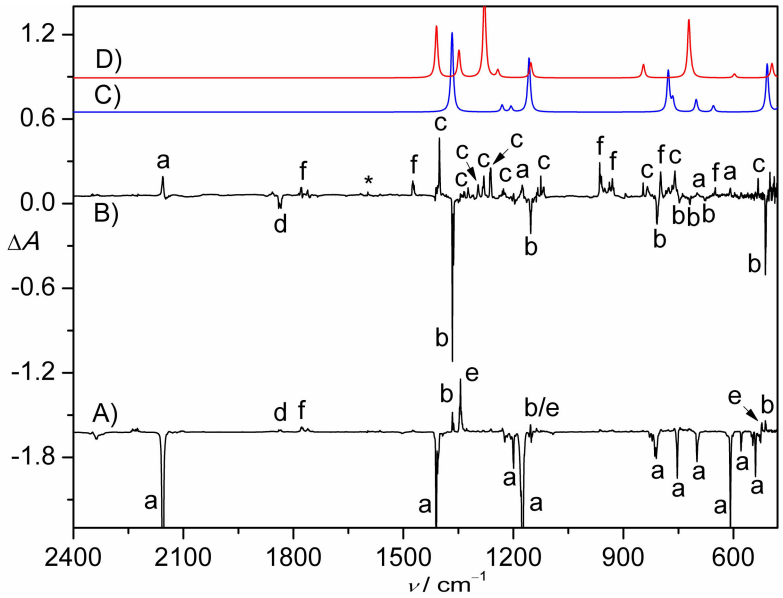

Figure 3. (**A**) IR difference spectrum (Absorbance, Δ*A*) showing the decomposition of $CHCl_2S(O)_2N_3$ in N_2-matrix upon a 193 nm laser photolysis (11 min); (**B**) IR difference spectrum (Absorbance, Δ*A*) showing the change of the N_2-matrix upon subsequent UV-light photolysis (365 nm, 10 min). (**C**) Calculated IR spectrum of triplet $CHCl_2S(O)_2N$ at the B3LYP/6-311++G(3df,3pd) level. (**D**) Calculated IR spectrum of $CHCl_2NSO_2$ (singlet-II) at the B3LYP/6-311++G(3df,3pd) level. The IR bands of $CHCl_2SO_2N_3$ (a), $CHCl_2SO_2N$ (b), $CHCl_2NSO_2$ (c), $CHCl_2S(O)NO$ (d), SO_2 (e), unknown species (f), and impurity H_2O (*) are labeled. For clarity, the spectra are arbitrarily shifted along the Δ*A* axis.

In order to distinguish these new IR bands, the matrix was irradiated with UV-light (365 nm), leading to the main depletion of the IR bands at 1835.1, 1366.5, 1153.2, 808.4, 747.7, 718.5, 675.8, and 512.6 cm^{-1} (Table 3). All these IR bands except the first one can be reasonably assigned to the nitrene intermediate $CHCl_2S(O)_2N$ in the triplet state by comparing with the calculated IR data (Figure 3C). With the aid of the calculations, weaker bands at 3027.2, 1196.1, and 1163.7 cm^{-1} were also found to belong to the same carrier. This assignment is further supported by the observation of well-resolved ^{15}N-isotopic shift of 9.6 cm^{-1} only for the S–N stretching mode (ν(SN)) at 718.5 cm^{-1}. As expected, the band position is very close to that in triplet $CH_2ClS(O)_2N$ at 718.9 cm^{-1}. As for the IR band at 1835.1 cm^{-1}, the accompanying large ^{15}N-isotopic shift of 31.7 cm^{-1} suggests a tentative assignment to an NO-containing species ($CHCl_2S(O)NO$, Table S5).

Table 3. Calculated and observed IR frequencies (>500 cm^{-1}) of $CHCl_2S(O)_2N$.

Calculated [a]				Observed [b]		Assignment [c]
Singlet		Triplet		N_2-matrix		
ν	Δν	ν	Δν	ν	Δν	
3167 (8)	0.0	3152 (6)	0.0	3027.2 (4)	<0.5	ν(CH)
1409 (139)	2.7	1367 (137)	0.0	1366.5 (100)	<0.5	$\nu_{asym}(SO_2)$
1225 (15)	0.0	1230 (11)	0.0	1196.1 (7)	<0.5	ϱ(CH)
1213 (5)	0.1	1206 (9)	0.0	1163.7 (4)	<0.5	ω(CH)
1048 (74)	10.0	1157 (93)	0.0	1153.2 (32)	<0.5	$\nu_{sym}(SO_2)$ + ω(CH)
978 (13)	11.1	777 (67)	0.2	808.4 (35)	<0.5	$\nu_{asym}(CCl_2)$
762 (100)	0.1	764 (24)	0.4	747.7 (16)	<0.5	$\nu_{sym}(CCl_2)$
760 (17)	0.6	701 (21)	10.7	718.5 (7)	9.6	ν(SN)
681 (13)	0.4	654 (10)	0.4	675.8 (5)	<0.5	ν(SC)
520 (101)	2.7	507 (82)	1.3	512.6 (50)	<0.5	$\delta(SO_2)$

[a] The calculated IR harmonic frequencies (ν, unscaled), ^{15}N-isotopic shifts (Δν), and band intensities (km mol^{-1}, in parentheses) for the singlet and triplet states at the B3LYP/6-311++G(3df,3pd) level. Full list of the calculated IR frequencies for all the conformers are given in Table S6. [b] The observed band positions (ν), ^{15}N-isotopic shifts (Δν), and relative intensities (in parentheses) in N_2-matrix. [c] Tentative assignment based on the calculated vibrational displacement vectors for the triplet state.

Upon the UV-light irradiation, $CHCl_2S(O)_2N$ partially recombines molecular nitrogen and reforms $CHCl_2S(O)_2N_3$ (Figure 3B). In the meantime, 1,2-$CHCl_2$ shift occurs and furnishes $CHCl_2NSO_2$ (Figure 3D). Similar to the IR spectrum of CH_2ClNSO_2 (Table 2), most of the IR bands for $CHCl_2NSO_2$ (Table 4) split into doublets due to weak interactions with the surrounding molecules. Based on the distinct ^{15}N-isotopic shifts, the IR bands at 1280.5/1262.7 and 1125.4/1117.0 cm^{-1} belong mainly to the ν(SN) and ν(CN) stretching modes, which are also very close to those in $CHCl_2NSO_2$ at 1283.7/1278.0 and 1114.6/1113.1 cm^{-1}, respectively. Additionally, another species with IR bands at 1777.3, 1474.4, 964.5, 930.5, and 798.8 cm^{-1} appears from the UV-light photolysis of $CHCl_2S(O)_2N$, its identification remains unclear.

Table 4. Calculated and observed IR frequencies (> 500 cm^{-1}) of $CHCl_2NSO_2$.

Calculated [a]				Observed [b]		Assignment [c]
Singlet-I		Singlet-II		N_2-matrix		
ν	Δν	ν	Δν	ν	Δν	
3151 (2)	0.0	3175 (1)	0.0			ν(CH)
1403 (190)	0.2	1409 (163)	0.0	1410.2/1401.7 (100)	<0.5	$\nu_{asym}(SO_2)$
1340 (7)	1.7	1348 (97)	9.1	1335.0/1323.8 (22)	<0.5	ϱ(CH)
1299 (431)	15.0	1278 (326)	7.8	1280.5/1262.7 (98)	16.0	ν(SN) + $\delta(SO_2)$
1252 (27)	0.0	1243 (25)	0.9	1230.2/1227.1 (7)	<0.5	ω(CH)
1129 (32)	15.3	1152 (52)	14.3	1125.4/1117.0 (35)	11.8	ν(CN) + $\nu_{sym}(SO_2)$
890 (44)	12.1	845 (47)	8.1	846.2/834.4 (33)	9.0	ν(CN)
758 (58)	1.4	721 (201)	1.0	783.9/776.9 (56)	<0.5	$\nu_{sym}(CCl_2)$
745 (169)	0.9	714 (18)	2.5	767.2/759.7 (40)	<0.5	$\nu_{asym}(CCl_2)$
526 (70)	1.8	597 (13)	8.5	532.5 (13)	2.2	$\delta(SO_2)$

[a] The calculated IR harmonic frequencies (ν, unscaled), ^{15}N-isotopic shifts (Δν), and band intensities (km mol^{-1}, in parentheses) at the B3LYP/6-311++G(3df,3pd) level. Full list of the calculated IR frequencies for all the conformers are given in Table S4. [b] The observed band positions (ν), ^{15}N-isotopic shifts (Δν), and relative intensities (in parentheses) in N_2-matrix. [c] Tentative assignment based on the calculated vibrational displacement vectors.

2.4. Flash Vacuum Pyrolysis of $CHCl_2S(O)_2N_3$

The IR spectrum of the flash vacuum pyrolysis (700 K) products of $CHCl_2S(O)_2N_3$ is depicted in Figure 4A. Traces of the azide survive, SO_2, HCN, HCl, CO, HNSO, $OCCl_2$ (m, 1817.9, 847.2 and 843.6 cm^{-1}) [40], ClCN (k, 2208.0 cm^{-1}) [41], $\bullet NSO_2$ (g, 1376.7, 1345.0, 1229.3 and 936.6 cm^{-1}) [27], $HNSO_2$ (l, 3329.6, 1387.9, 1300.3, and 672.1 cm^{-1}) [26], and $\bullet CHCl_2$ (h, 1223.3 and 896.2 cm^{-1}) [42] can be identified among the pyrolysis products. The identification of $\bullet NSO_2$ can be ascertained with the subsequent photoisomerization with OSNO• upon further UV-light irradiation (Figure 4B).

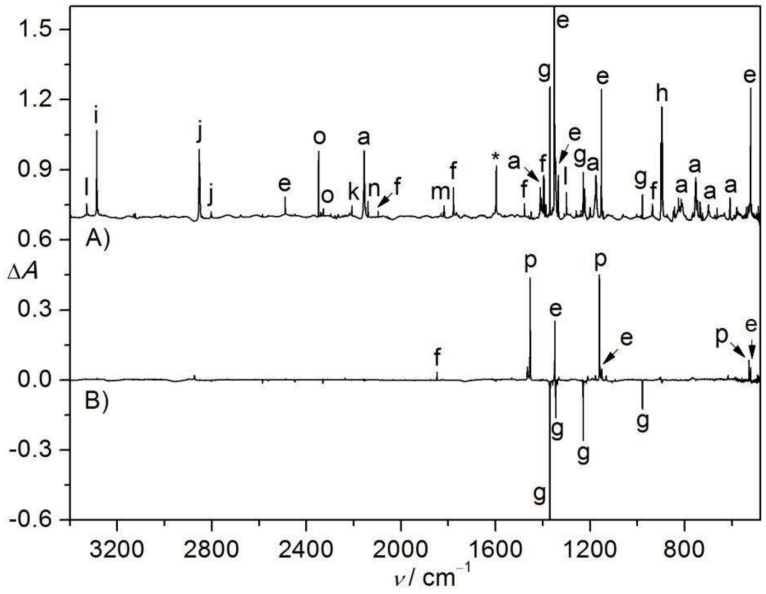

Figure 4. (**A**) IR spectrum (Absorbance, *A*) of the N_2-matrix isolated flash vacuum pyrolysis (700 K) products of $CHCl_2S(O)_2N_3$. (**B**) IR difference spectrum (Absorbance, ΔA) showing the change of the N_2-matrix upon subsequent UV-light photolysis (365 nm, 10 min). The IR bands of $CHCl_2SO_2N_3$ (a), SO_2 (e), unknown species (f), $\bullet NSO_2$ (g), $CHCl_2$ (h), HCN (i), HCl (j), ClCN (k), $HNSO_2$ (l), $OCCl_2$ (m), CO (n), CO_2 (o), OSNO (p), and impurity H_2O (*) are labeled. For clarity, the spectra are arbitrarily shifted along the ΔA axis.

The presence of $\bullet NSO_2$ and $\bullet CHCl_2$ but no counterpart $\bullet N_3$ radicals among the FVP products of $CHCl_2S(O)_2N_3$ clearly demonstrates that the azide decomposes by the first formation of $CHCl_2S(O)_2N$ through N_2-elimination. However, the initially generated nitrene $CHCl_2S(O)_2N$ is thermally unstable, which dissociates by homolytic cleavage of the C–S bond. Alternatively, it may undergo heterolytic cleavage of the C–S bond with concerted H-migration to furnish $HNSO_2$ and dichlorocarbene CCl_2, and the latter reacts with oxygen-containing species and yields the experimentally observed $OCCl_2$. Another possible pathway involves the isomerization of $CHCl_2S(O)_2N$ to $CHCl_2NSO_2$, and the latter may break the C–N bond to a pair of radicals $\bullet NSO_2/\bullet CHCl_2$ and $HNSO_2/CCl_2$. It should be noted that the FVP of $CHCl_2S(O)_2N_3$ provides an efficient and practical method for the gas-phase generation of the atmospherically-important radical $\bullet CHCl_2$ [43], since its production in the previous spectroscopic studies utilized either laser photolysis of $CHCl_2Br$ [44] or the reaction of chloroform with lithium atoms [45].

2.5. EPR Spectroscopy

To capture the nitrene intermediates in the decomposition of $CH_2ClS(O)_2N_3$ and $CHCl_2S(O)_2N_3$, the photochemistry (266 nm) of both sulfonyl azides in glassy toluene matrices (5 K) was followed with EPR spectroscopy. The obtained EPR spectra (Figure 5) demonstrate typical triplet nitrene signals in the region of 7500–9000 G at about 9.40 GHz resonance frequency. The derived zero-field splitting parameters (ZFSP) for $CH_2ClS(O)_2N$ ($|D/hc|$ = 1.57 cm^{-1} and $|E/hc|$ = 0.0026 cm^{-1})

and $CHCl_2S(O)_2N$ ($|D/hc|$ = 1.56 cm^{-1} and $|E/hc|$ = 0.0042 cm^{-1}) are very similar to those of other sulfonyl nitrenes, such as $Me_2NS(O)_2$–N ($|D/hc|$ = 1.57 cm^{-1} and $|E/hc|$ = 0.0038 cm^{-1}) [46], $CF_3S(O)_2$–N ($|D/hc|$ = 1.741 cm^{-1} and $|E/hc|$ = 0 cm^{-1}) [12], and $FS(O)_2N$ ($|D/hc|$ = 1.620 cm^{-1} and $|E/hc|$ = 0.0055 cm^{-1}) [13]. According to the linear correlation between the calculated spin densities (ϱ, $CH_2ClS(O)_2N$: 1.92; $CHCl_2S(O)_2N$: 1.91, M06-2X/6-311++G(3df,3pd)) and zero-field D values [47,48], the predicted D values of 1.72 and 1.70 cm^{-1} agree with the experimental observations of 1.57 and 1.56 cm^{-1}, respectively. Consistent with the observed nonzero E values in $CH_2ClS(O)_2$–N and $CHCl_2S(O)_2$–N, small spin densities of about 0.12 are equally distributed on the two neighboring O atoms.

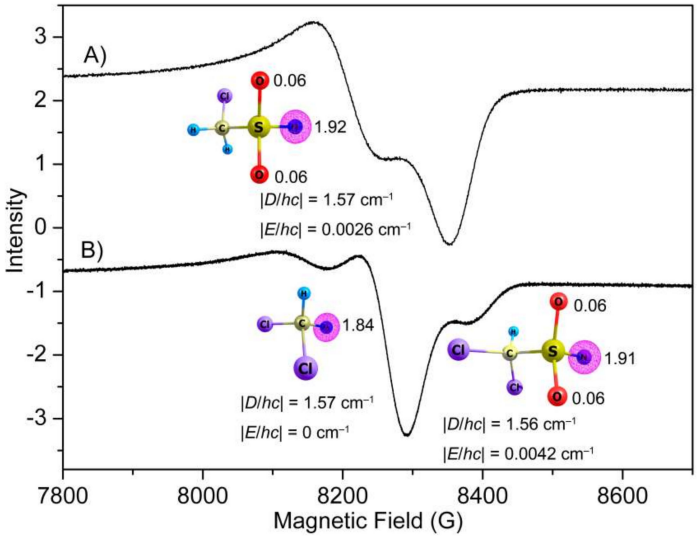

Figure 5. EPR spectra of the 266 nm laser photolysis products of $CH_2ClS(O)_2N_3$ (**A**) and $CHCl_2S(O)_2N_3$ (**B**) in glassy toluene matrices (0.4 mmol mL^{-1}) at 5 K. Natural spin densities of the nitrenes computed at the M06-2X/6-311++G(3df,3pd) level are depicted.

In line with the IR spectroscopic observation of SO_2-elimination during the photolysis of $CHCl_2S(O)_2N_3$, a second triplet nitrene signal with ZFSP of $|D/hc|$ = 1.57 cm^{-1} and $|E/hc|$ = 0 cm^{-1} for dichloromethylnitrene $CHCl_2N$ was also observed in the EPR spectrum (Figure 5B). Its assignment is supported by the close similarity with other alkyl nitrenes such as CH_3N ($|D/hc|$ = 1.720 cm^{-1} and $|E/hc|$ < 0.003 cm^{-1}) [49] and CF_3N ($|D/hc|$ = 1.741 cm^{-1} and $|E/hc|$ = 0 cm^{-1}) [12]. In contrast, no EPR signal for chloromethylnitrene CH_2ClN could be observed in the photolysis of $CH_2ClS(O)_2N_3$, which is probably due to immediate isomerization to singlet species (CHCl=NH) under the photolysis conditions.

2.6. Quantum Chemical Calculations

The energies for the species involving in the stepwise decomposition of $CH_2ClS(O)_2N_3$ and $CHCl_2S(O)_2N_3$ via the intermediacy of the corresponding nitrenes were calculated at the B3LYP/6-311++G(3df,3pd) level (Figure 6). The barriers (TS1) for the N_2-elimination in $CH_2ClS(O)_2N_3$ (35.3 kcal mol^{-1}) and $CHCl_2S(O)_2N_3$ (34.8 kcal mol^{-1}) are comparable with those of other sulfonyl azides such as $PhS(O)_2N_3$ (35 kcal mol^{-1}, CBS-QB3) [28] and $CH_3OS(O)_2N_3$ (35 kcal mol^{-1}, CCSD(T)/6-311++G(2df,2p)//UMP2/6-311++G(2df,2p)) [26], and they are also close to those for the nitrene formation in typical carbonyl azides such as $FC(O)N_3$ (33 kcal mol^{-1}, B3LYP/6-311+G(3df)) [50] and $CH_3OC(O)N_3$ (34 kcal mol^{-1}, B3LYP/6-311++G(3df,3pd)) [51].

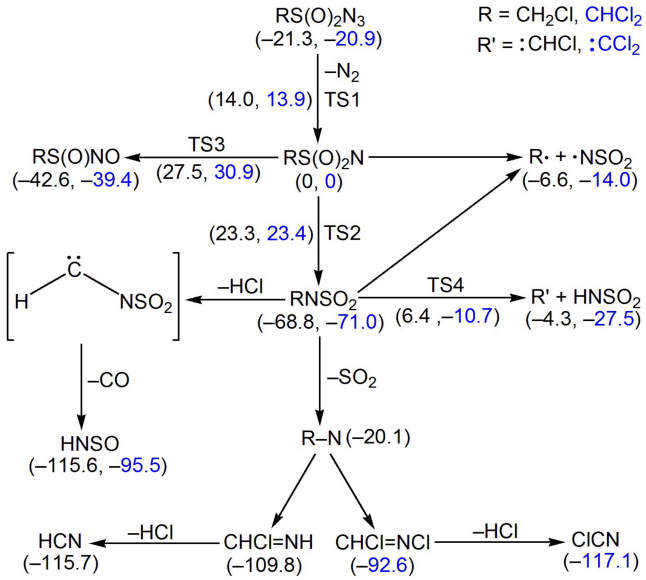

Figure 6. Calculated energy profile for the decomposition of $RS(O)_2N_3$ (R = CH_2Cl and $CHCl_2$) in the singlet state at the B3LYP/6-311++G(3df,3pd) level of theory. The calculated molecules structures (bond lengths in Å and angles in °) for the selected species are also depicted.

For the initially-generated singlet sulfonyl nitrenes $RS(O)_2N$ (R = CH_2Cl and $CHCl_2$), several competing processes might be responsible for their disappearance. Similar to the well-established Curtius-rearrangement of all carbonyl nitrenes (RC(O)N → RNCO) [52], $RS(O)_2N$ can undergo either 1,2-R shift to $RNSO_2$ or 1,2-oxygen shift to RS(O)NO. Both pathways are highly exothermic, and the higher activation barriers for the latter (TS3, $CH_2ClS(O)_2N$: 27.5 kcal mol^{-1}; $CHCl_2S(O)_2N$: 30.9 kcal mol^{-1}) than the former (TS2, $CH_2ClS(O)_2N$: 23.3 kcal mol^{-1}; $CHCl_2S(O)_2N$: 23.4 kcal mol^{-1}) render their contribution in the gas phase reactions of the nitrenes unlikely. However, the excessive energy input from the ArF laser irradiation (193 nm, 148 kcal mol^{-1}) [53] in the photochemistry can overcome the barrier and enable the formation of RS(O)NO as minor products. In addition to the intramolecular rearrangement, the sulfonyl nitrenes may decompose exothermically through the homolytic C–S bond cleavage to alkyl radicals R• (•CH_2Cl and •$CHCl_2$) and •NSO_2 or heterolytic C–N bond fragmentation with concerted H-migration to carbenes HCCl and ClCCl and $HNSO_2$. These two pairs of fragments may also be derived from the decomposition of $RNSO_2$; however, the large C–N bond dissociation energies (CH_2ClNSO_2: 62.2 kcal mol^{-1}; $CHCl_2NSO_2$: 57.0 kcal mol^{-1}) and formidable barriers for the concerted H-migration (TS4, CH_2ClNSO_2: 75.2 kcal mol^{-1}; $CHCl_2NSO_2$: 60.3 kcal mol^{-1}) rule out these pathways under the pyrolysis conditions. In agreement with the IR detectable amounts of •$CHCl_2$/•NSO_2 and $OCCl_2$/$HNSO_2$ among the FVP products of $CHCl_2S(O)_2N_3$, the energy release from the decomposition of $CHCl_2S(O)_2N$ is larger than that of $CHCl_2NSO_2$.

The absence of $RNSO_2$ (R = CH_2Cl and $CHCl_2$), but the presence of HCl, CO, and HNSO, among the pyrolysis products of the azides implies further dissociation through the thermodynamically favorable HCl- or Cl_2-elimination (Figure 6). According to the B3LYP/6-311++G(3df,3pd) calculation, the putative carbene species H–C–NSO_2 is highly unstable in the closed-shell singlet state and prefers either N–S bond breakage to HCN and SO_2 or further CO-elimination to HNSO. The SO_2 formation may also be attributed to the direct N–S bond breakage in $RNSO_2$. By analogy to the thermal instability of other alkyl nitrenes (e.g., CH_3N [54] and CF_3N [12]), the thermally-generated nitrenes CH_2ClN and $CHCl_2N$ isomerize to CHCl=NH and CHCl=NCl and then eliminate HCl to yield the observed HCN and ClCN, respectively.

The calculated molecular structures and relative energies of $CH_2ClS(O)_2N$ and $CHCl_2S(O)_2N$ in the singlet and triplet states are depicted in Figure 7. For each nitrene in the singlet state, three rotamers differing in the staggered orientation of the methyl group with respect to the SO_2N moiety

are close-in-energy minima. Consistent with the IR and EPR spectroscopic observations, both sulfonyl nitrenes prefer triplet ground state, and the singlet state are about 15 kcal mol^{-1} higher in energy at the B3LYP/6-311++G(3df,3pd) level. The energy gaps between the singlet and triplet states (ΔE_{ST}) for $CH_2ClS(O)_2N$ (15.1 kcal mol^{-1}) and $CHCl_2S(O)_2N$ (14.5 kcal mol^{-1}) are close to those of $CH_3S(O)_2N$ (13.6 kcal mol^{-1}) and $PhS(O)_2N$ (14.7 kcal mol^{-1}) at the same theoretical level [31].

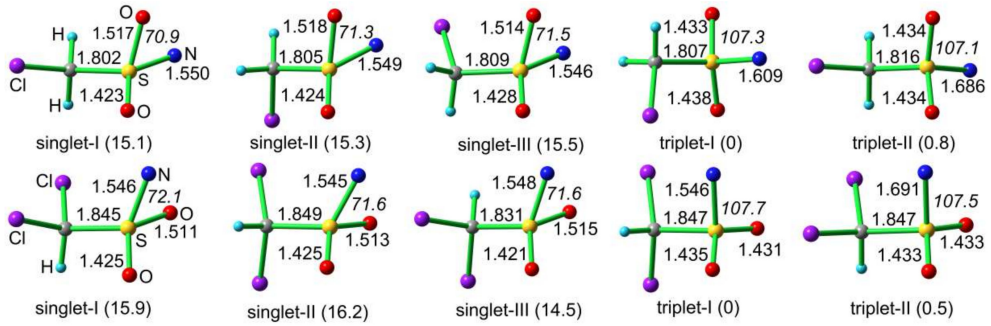

Figure 7. Calculated molecular structures and relative energies (in parentheses, kcal mol^{-1}) of $CH_2ClS(O)_2N$ and $CHCl_2S(O)_2N$ at the B3LYP/6-311++G(3df,3pd) level. Selected bond lengths in Å and angles in ° (in italics) are given.

Due to intramolecular interaction between the oxygen atom with the electron-deficient nitrogen center, the singlet sulfonyl nitrenes are distorted from C_s-symmetry. In the lowest-energy C_1-symmetric rotamer (singlet-I) of $CH_2ClS(O)_2N$, the Cl–C and S–N bonds adopts an antiperiplanar configuration with a dihedral angle (φ(ClCSN)) of −158.8°. The φ(ClCSN) dihedral angles in singlet-II and singlet-III are 84.4 and −31.7°, respectively. Similarly, in the most stable rotamer of singlet $CHCl_2S(O)_2N$ (singlet-III), the two S–N bond adopts an antiperiplanar configuration with the bisector of the ClSCl angle. In the triplet state of $CH_2ClS(O)_2N$, the more stable rotamer (triplet-I) adopts C_1-symmetry with the S–N bond being synperiplanar with the Cl–C bond (φ(ClCSN) = −63.3°); however, the C_s-symmetric rotamer (triplet-II) exhibits an synperiplanar conformation between these two bonds (φ(ClCSN) = 180°). Structurally, sulfonyl nitrenes in the singlet state are stabilized by the intramolecular N–O interactions, as evidenced by the considerably smaller OSN angles in the singlet state (ca. 72°) than the triplet state (ca. 107°). Unlike the much stronger intramolecular N–N interactions in singlet ground-state sulfamoyl nitrenes [46], the stabilizing N–O interactions in alkylsulfonyl nitrenes can hardly switch the spin-state. In contrast, very recent studies on structurally-related carbonyl nitrenes RC(O)N have demonstrated that the spin multiplicity can be effectively switched by the stabilizing N–O interactions [18,52].

3. Materials and Methods

3.1. Sample Preparation

Caution! Covalent azides are explosive! Although no explosions occurred during this work, appropriate safety precautions (face shields, leather gloves, and protective leather clothing) should be taken, especially when working with pure $CH_2ClS(O)_2N_3$ and $CHCl_2S(O)_2N_3$ in the condensed phase.

Chloromethylsulfonyl azide, $CH_2ClS(O)_2N_3$, was prepared by the reaction of chloromethylsulfonyl chloride with sodium azide. Briefly, acetonitrile (0.3 mL) and freshly purified chloromethylsulfonyl chloride (0.3 g, 2.0 mmol) were distilled into a glass vessel which contains dried NaN_3 (0.2 g, 3.2 mmol). The mixture was stirred at room temperature for 18 h. The volatile crude products were separated by passing through three successive cold U-traps (−20, −80, and −196 °C). Pure azide $CH_2ClS(O)_2N_3$ was retained in the first trap as white crystals. ^{1}H-NMR (400MHz, $CDCl_3$, 298 K): δ = 4.72 (s, 2H); ^{13}C-NMR (400 MHz, $CDCl_3$ 298 K): δ = 57.9 ppm; IR (gas-phase): 2148, 1412, 1246, 1183, 1135, 868, 814, 750, 577, and 524 cm^{-1}; Raman(solid): 3032, 2961,

2161, 1391, 1185, 1163, 1131, 869, 807, 747, 736, 575, 536, 515, 451, 407, 315, and 285 cm^{-1}. 1-^{15}N sodium azide (98 atom% ^{15}N, EURISO-TOP GmbH) was used for the preparation of ^{15}N-labeled sample.

Dichloromethylsulfonyl azide, $CHCl_2S(O)_2N_3$, was synthesized in a similar manner by the reaction of freshly purified dichloromethylsulfonyl chloride (0.6 g, 3.0 mmol) with NaN_3 (0.3 g, 4.6 mmol) in acetonitrile (0.5 mL). The mixture was stirred at room temperature for 24 h. Separation of the volatile products was carried out by using three cold traps of −16, −80, and −196 °C. The desired product $CHCl_2S(O)_2N_3$ was retained in the first trap as colorless liquid. ^{1}H-NMR (400 MHz, $CDCl_3$, 298 K): δ = 6.41 ppm (s, 1H); ^{13}C-NMR (400 MHz, $CDCl_3$, 298 K): δ = 79.4 ppm; IR (gas-phase): 2148, 1422, 1355, 1222, 1179, 1150, 816, 751, 694, 608, 576, and 529 cm^{-1}; Raman (liquid): 2993, 2961, 2155, 1382, 1203, 1156, 1144, 799, 746, 698, 603, 575, 536, 452, 410, 342, 295, 238, and 211 cm^{-1}. 1-^{15}N sodium azide (98 atom % ^{15}N, EURISO-TOP GmbH) was used for the preparation of ^{15}N labeled sample.

3.2. Spectroscopy

Gas-phase IR spectra were recorded on a Bruker spectrometer (Tensor 27) (Bruker Optik GmbH, Ettlingen, Germany). Raman spectra were recorded on a Horiba JY HR800 Raman spectroscopy (HORIBA, Lille, France).

3.3. Matrix IR Spectroscopy

Matrix IR spectra were recordedon a FT-IR spectrometer (Bruker 70 V) in a reflectance mode using a transfer optic. A KBr beam splitter and MCT detector were used in the mid-IR region (4000−500 cm^{-1}). For each spectrum, 200 scans at a resolution of 0.5 cm^{-1} were coadded. The gas sample mixed by passing a flow of N_2 gas through a cold U-trap ($CH_2ClS(O)_2N_3$: −5 °C; $CHCl_2S(O)_2N_3$: −10 °C) containing ca. 10 mg of the azide. The mixture (azide/dilution gas ≈ 1:1000 estimated) was passed through an aluminum oxide (o.d. 2.0 mm, i.d. 1.0 mm), which could be heated over a length of approximately 25 mm by a tantalum wire (o.d. 0.4 mm, resistance 0.4 Ω). Then, the mixture was immediately deposited (2 mmol/h) onto the Rh-plated copper block matrix support (15 K) in a high vacuum (~10^{-6} Pa). While not directly measured, the expected residence time of the mixture in the pyrolysis tube is about a few milliseconds, and the pressure inside the pyrolysis tube is about 10 mbar. The electric power (voltage/current) used in pyrolysis experiments was 4.0 V/1.9 A for $CH_2ClS(O)_2N_3$ and 4.5 V/2.9 A for $CHCl_2S(O)_2N_3$. Photolysis experiments were performed with ArF excimer laser (GAM LASER, Orlando, FL, USA) (193 nm, Gamlaser EX5/250, 5 mJ, 3 Hz), Nd^{3+}: YAG laser (266 nm, MPL-F-266, 10 mW), and UV lamp (365 nm).

3.4. Computational Details

Geometry optimizations were performed using DFT-B3LYP [55] method combined with the 6-311++G(3df,3pd) basis set. Time-dependent (TD) DFT (B3LYP/6-311++G(3df,3pd)) [56,57] calculations were performed for the prediction of UV−vis transitions. Local minima were confirmed by vibrational frequency analysis, and transition states were further confirmed by intrinsic reaction coordinate (IRC) calculations [58,59]. All the calculations were performed using the Gaussian 09 software package (Gaussian, Inc., Wallingford, CT, USA) [60].

4. Conclusions

The UV laser photolytic (193 and 266 nm) and thermal decomposition of two alkylsulfonyl azides $RS(O)_2N_3$ (R = CH_2Cl and $CHCl_2$) have been studied by combining matrix-isolation IR and EPR spectroscopy and quantum chemical calculations. Two new sulfonyl nitrenes $CH_2ClS(O)_2N$ and $CHCl_2S(O)_2N$ in the triplet ground state have been directly observed and spectroscopically characterized. Upon subsequent UV light irradiations, both nitrenes undergo rearrangement reactions to the corresponding *N*-sulfonlyamines R–NSO_2 and 1,2-oxygen shift to *S*-nitroso compounds R–S(O)NO in solid N_2-matrices. In the gas phase, the monochloro-substituted sulfonyl nitrene $CH_2ClS(O)_2N$ prefers rearrangement to CH_2ClNSO_2 with subsequent decomposition to

HCl, HNSO, and CO, in which an intriguing carbene species H–C–NSO_2 might be involved. The dichloro-substituted sulfonyl nitrene $CHCl_2S(O)_2N$ partially undergoes homolytic C–S bond cleavage to a pair of radicals •$CHCl_2$ and •NSO_2. Its rearrangement product $CHCl_2NSO_2$ also decomposes to $HNSO_2/CCl_2$ and $HCl/SO_2/ClCN$.

Supplementary Materials: The following are available online. Calculated vertical transitions, structures, energies and IR frequencies, and Calculated atomic coordinates for all optimized structures.

Author Contributions: Conceptualization, X.Z.; Methodology, Y.Y., X.C., M.A., and X.Z.; Software, X.C., Y.L., and M.A.; Formal Analysis, X.Z., Y.Y., Y.L., and X.C.; Writing, X.Z. and Y.Y.; Supervision, X.Z.

Funding: This work was supported by the National Natural Science Foundation of China (21673147, 21422304) and the project of scientific and technologic infrastructure of Suzhou (SZS201708).

Conflicts of Interest: The authors declare no conflict of interest.

References

1. Gritsan, N.P. *Properties of Carbonyl Nitrenes and Related Acyl Nitrenes. Nitrenes and Nitrenium Ions*, 1st ed.; Falvey, D.E., Gudmundsdottir, A.D., Eds.; John Wiley & Sons, Inc.: Hoboken, NJ, USA, 2013; Volume 6, pp. 481–548. ISBN 978-0-470-39059-7.
2. Jiang, H.L.; Lang, K.; Lu, H.J.; Wojtas, L.; Zhang, X.P. Intramolecular radical aziridination of allylic sulfamoyl azides by cobalt(II)-based metalloradical catalysis: Effective construction of strained heterobicyclic structures. *Angew. Chem. Int. Ed.* **2016**, *55*, 11604–11608. [CrossRef] [PubMed]
3. Lu, H.J.; Li, C.Q.; Jiang, H.L.; Lizardi, C.L.; Zhang, X.P. Chemoselective amination of propargylic C(sp^3)-H bonds by cobalt(II)-based metalloradical catalysis. *Angew. Chem. Int. Ed.* **2014**, *126*, 7148–7152. [CrossRef]
4. Liu, L.-H.; Yan, M. Perfluorophenyl azides: New applications in surface functionalization and nanomaterial synthesis. *Acc. Chem. Res.* **2010**, *43*, 1434–1443. [CrossRef] [PubMed]
5. Lwowski, W. Nitrenes and the decomposition of carbonylazides. *Angew. Chem. Int. Ed.* **1967**, *6*, 897–1012. [CrossRef]
6. Kundu, S.; Miceli, E.; Farquhar, E.; Pfaff, F.F.; Kuhlmann, U.; Hildebrandt, P.; Braun, B.; Greco, C.; Ray, K. Lewis acid trapping of an elusive copper−tosylnitrene intermediate using scandium triflate. *J. Am. Chem. Soc.* **2012**, *134*, 14710–14713. [CrossRef] [PubMed]
7. Gritsan, N.P.; Likhotvorik, I.; Tsao, M.-L.; Celebi, N.; Platz, M.S.; Karney, W.L.; Kemnitz, C.R.; Borden, W.T. Ring-expansion reaction of cyano-substituted singlet phenyl nitrenes: Theoretical predictions and kinetic results from laser flash photolysis and chemical trapping experiments. *J. Am. Chem. Soc.* **2001**, *123*, 1425–1433. [CrossRef]
8. Kubicki, J.; Luk, H.L.; Zhang, Y.; Vyas, S.; Peng, H.-L.; Hadad, C.M.; Platz, M.S. Direct observation of a sulfonyl azide excited state and its decay processes by ultrafast time-resolved IR Spectroscopy. *J. Am. Chem. Soc.* **2012**, *134*, 7036–7044. [CrossRef] [PubMed]
9. Kuzmin, A.V.; Neumann, C.; van Wilderen, L.J.G.W.; Shainyanb, B.A.; Bredenbeck, J. Exploring photochemistry of p-bromophenylsulfonyl, p-toylsulfonyl and methylsulfonyl azides by ultrafast UV-Pump-IR-Probe spectroscopy and computations. *Phys. Chem. Chem. Phys.* **2016**, *18*, 8662–8672. [CrossRef] [PubMed]
10. Kubicki, J.; Zhang, Y.; Xue, J.; Luk, H.L.; Platz, M.S. Ultrafast time resolved studies of the photochemistry of acyl and sulfonyl azides. *Phys. Chem. Chem. Phys.* **2012**, *14*, 10377–10390. [CrossRef]
11. Zeng, X.Q.; Beckers, H.; Willner, H. Thermally persistent fluorosulfonyl nitrene and unexpected formation of the fluorosulfonyl radical. *J. Am. Chem. Soc.* **2013**, *135*, 2096–2099. [CrossRef]
12. Zeng, X.Q.; Beckers, H.; Willner, H.; Neuhaus, P.; Grote, D.; Sander, W. Photochemistry of matrix isolated (trifluoromethyl)sulfonyl azide, $CF_3SO_2N_3$. *J. Phys. Chem. A* **2015**, *119*, 2281–2288. [CrossRef]
13. Zeng, X.Q.; Beckers, H.; Neuhaus, P.; Grote, D.; Sander, W. Elusive fluoro sulfinyl nitrite, FS(O)NO, produced by photolysis of matrix-isolated $FS(O)_2N$. *Z. Anorg. Allg. Chem.* **2012**, *638*, 526–533. [CrossRef]
14. Obenhuber, A.H.; Gianetti, T.L.; Berrebi, X.; Bergman, R.G.; Arnold, J. Reaction of (bisimido)niobium(V) complexes with organic azides: [3+2] cycloaddition and reversible cleavage of β-diketiminato ligands involving nitrene transfer. *J. Am. Chem. Soc.* **2014**, *136*, 2994–2997. [CrossRef] [PubMed]

15. Klima, R.F.; Gudmundsdottir, A.D. Intermolecular triplet-sensitized photolysis of alkyl azides trapping of triplet alkyl nitrenes. *J. Photochem. Photobiol. A.* **2004**, *162*, 239–247. [CrossRef]
16. Hayes, J.C.; Sheridan, R.S. Infrared spectrum of triplet phenylnitrene. On the origin of didehydroazepine in low-temperature matrices. *J. Am. Chem. Soc.* **1990**, *112*, 5879–5881. [CrossRef]
17. Leyva, E.; Platz, M.S.; Persy, G.; Wirz, J. Photochemistry of phenyl azide: The role of singlet and triplet phenylnitrene as transient intermediates. *J. Am. Chem. Soc.* **1986**, *108*, 3783–3790. [CrossRef]
18. Kubicki, J.; Zhang, Y.; Vyas, S.; Burdzinski, G.; Luk, H.L.; Wang, J.; Xue, J.; Peng, H.-L.; Pritchina, E.A.; Sliwa, M.; et al. Photochemistry of 2-naphthoyl azide. An ultrafast time-resolved UV-vis and IR spectroscopic and computational Study. *J. Am. Chem. Soc.* **2011**, *133*, 9751–9761. [CrossRef] [PubMed]
19. Vyas, S.; Kubicki, J.; Luk, H.L.; Zhang, Y.; Gritsan, N.P.; Hadad, C.M.; Platz, M.S. An ultrafast time-resolved infrared and UV-vis spectroscopic and computational study of the photochemistry of acyl azides. *J. Phys. Org. Chem.* **2012**, *25*, 693–703. [CrossRef]
20. Zeng, X.Q.; Beckers, H.; Willner, H.; Grote, D.; Sander, W. The missing link: Triplet fluorocarbonyl nitrene FC(O)N. *Chem. Eur. J.* **2011**, *17*, 3977–3984. [CrossRef]
21. Chuprakov, S.; Worrell, B.T.; Selander, N.; Sit, R.K.; Fokin, V.V. Stereoselective 1,3-insertions of rhodium(II) azavinyl carbenes. *J. Am. Chem. Soc.* **2014**, *136*, 195–202. [CrossRef]
22. McIntosh, J.A.; Coelho, P.S.; Farwell, C.C.; Wang, Z.J.; Lewis, J.C.; Brown, T.R.; Arnold, F.H. Enantioselective intramolecular C-H amination catalyzed by engineered cytochrome P450 enzymes in vitro and in vivo. *Angew. Chem. Int. Ed.* **2013**, *125*, 9479–9482. [CrossRef]
23. Lu, H.J.; Jiang, H.L.; Wojtas, L.; Zhang, X.P. Selective intramolecular C-H amination through the metalloradical activation of azides: Synthesis of 1,3-diamines under neutral and nonoxidative conditions. *Angew. Chem. Int. Ed.* **2010**, *122*, 10390–10394. [CrossRef]
24. Lwowski, W.; Scheiffele, E. Curtius and lossen rearrangements. I. The benzenesulfonyl system. *J. Am. Chem. Soc.* **1965**, *87*, 4359–4365. [CrossRef]
25. Sheridan, R.S.; Rempala, P. Books of Abstracts. In Proceedings of the 217th ACS National Meeting, Anaheim, CA, USA, 21–25 March 1999; American Chemical Society: Washington, DC, USA, 1999.
26. Deng, G.H.; Wu, Z.; Li, D.Q.; Linguerri, R.; Francisco, J.S.; Zeng, X.Q. Simplest *N*-sulfonylamine $HNSO_2$. *J. Am. Chem. Soc.* **2016**, *138*, 11509–11512. [CrossRef] [PubMed]
27. Zeng, X.Q.; Beckers, H.; Willner, W. The iminyl radical O_2SN. *Angew. Chem. Int. Ed.* **2013**, *52*, 7981–7984. [CrossRef] [PubMed]
28. Deng, G.H.; Dong, X.L.; Liu, Q.F.; Li, D.Q.; Li, H.M.; Sun, Q.; Zeng, X.Q. The decomposition of benzenesulfonyl azide: A matrix isolation and computational study. *Phys. Chem. Chem. Phys.* **2017**, *19*, 3792–3799. [CrossRef] [PubMed]
29. Weidner, K.; Giroult, A.; Panchaud, P.; Renaud, P. Efficient carboazidation of alkenes using a radical desulfonylative azide transfer process. *J. Am. Chem. Soc.* **2010**, *132*, 17511–17515. [CrossRef] [PubMed]
30. Wu, Z.; Wan, H.B.; Xu, J.; Lu, B.; Lu, Y.; Eckhardt, A.K.; Schreiner, P.R.; Xie, C.J.; Guo, H.; Zeng, X.Q. The near-UV absorber OSSO and its isomers. *Chem. Commun.* **2018**, *54*, 4517–4520. [CrossRef] [PubMed]
31. Deng, G.H.; Li, D.Q.; Wu, Z.; Li, H.M.; Bernhardt, E.; Zeng, X.Q. Methanesulfonyl azide: Molecular structure and photolysis in solid noble gas matrices. *J. Phys. Chem. A* **2016**, *120*, 5590–5597. [CrossRef]
32. Lu, Y.; Li, H.M.; Wan, H.B.; Liu, Q.; Deng, G.H.; Zeng, X.Q. Flash vacuum pyrolysis of sulfamoyl azides and chlorides: Facile gas-hhase generation of transient *N*-sulfonylamines. *J. Anal. Appl. Pyrolysis.* **2018**, *134*, 476–483. [CrossRef]
33. Schriver-Mazzuoli, L.; Chaabouni, H.; Schriver, A. Infrared spectra of SO_2 and SO_2: H_2O ices at low temperature. *J. Mol. Struct.* **2003**, *644*, 151–164. [CrossRef]
34. Allavena, M.; Rysnik, R.; White, D.; Calder, V.; Mann, D.E. Infrared spectra and geometry of SO_2 isotopes in solid krypton matrices. *J. Chem. Phys.* **1969**, *50*, 3399–3410. [CrossRef]
35. Hooper, N.; Beeching, L.J.; Dyke, J.M.; Morris, A.; Ogden, J.S. A study of the thermal decomposition of 2-azidoethanol and 2-azidoethyl acetate by ultraviolet photoelectron spectroscopy and matrix isolation infrared spectroscopy. *J. Phys. Chem. A* **2002**, *106*, 9968–9975. [CrossRef]
36. Wu, Z.; Liu, Q.F.; Li, D.Q.; Feng, R.J.; Zeng, X.Q. Flash vacuum pyrolysis of methoxysulfinyl azide: Stepwise decomposition via methoxysulfinyl nitrene. *J. Anal. Appl. Pyrolysis.* **2017**, *124*, 610–617. [CrossRef]
37. Zeng, X.Q.; Bernhardt, E.; Beckers, H.; Banert, K.; Hagedorn, M.; Liu, H.L. Formyl azide: Properties and solid-state structure. *Angew. Chem. Int. Ed.* **2013**, *52*, 3503–3506. [CrossRef] [PubMed]

38. d'Hendecourt, L.B.; Grim, R.J.A. Time-dependent chemistry in dense molecular clouds. *Astron. Astrophys.* **1986**, *167*, 161–165.
39. Nonella, M.; Huber, J.R.; Ha, T.K. Photolytic preparation and isomerization of HNSO, HOSN, HSNO, and HONS in an argon matrix. An experimental and theoretical study. *J. Phys. Chem.* **1987**, *91*, 5203–5209. [CrossRef]
40. Tobón, Y.A.; Nieto, L.I.; Romano, R.M.; Della Védova, C.O.; Downs, A.J. Photochemical reaction channels of OCS with Cl_2, ICl, or IBr isolated together in an argon matrix: Isolation of syn-iodocarbonylsulfenyl bromide. *J. Phys. Chem. A* **2006**, *110*, 2674–2681. [CrossRef]
41. Ramos, L.A.; Zeng, X.Q.; Ulic, S.E.; Beckers, H.; Willner, H.; Della Védova, C.O. Chlorodifluoroacetyl azide, $ClF_2CC(O)N_3$: Preparation, Properties, and Decomposition. *J. Org. Chem.* **2012**, *77*, 6456–6462. [CrossRef]
42. Fridgen, T.D.; Zhang, X.K.; Parnis, J.M.; March, R.E. Isomerization and fragmentation products of CH_2Cl_2 and other dihalomethanes in rare-gas matrices: An electron bombardment matrix-isolation FTIR spectroscopic study. *J. Phys. Chem. A* **2000**, *104*, 3487–3497. [CrossRef]
43. Tsang, W. Mechanisms for the formation and destruction of chlorinated organic products of incomplete combustion. *Combust. Sci. Technol.* **1990**, *74*, 99–116. [CrossRef]
44. Yang, S.X.; Hou, G.Y.; Dai, J.H.; Chang, C.H.; Chang, B.C. Spectroscopic investigation of the multiphoton photolysis reactions of bromomethanes ($CHBr_3$, $CHBr_2Cl$, $CHBrCl_2$, and CH_2Br_2) at near-ultraviolet wavelengths. *J. Phys. Chem. A* **2010**, *114*, 4785–4790. [CrossRef] [PubMed]
45. Carver, T.G.; Andrews, L. Matrix infrared spectrum and bonding in the dichloromethyl radical. *J. Chem. Phys.* **1969**, *50*, 4235–4245. [CrossRef]
46. Lu, Y.; Li, H.M.; Abe, M.; Bégué, D.; Wan, H.B.; Deng, G.H.; Xu, J.; Liu, K.; Zeng, X.Q. Sulfamoyl nitrenes: Singlet or triplet ground state? *Chem. Commun.* **2018**, *54*, 6136–6139. [CrossRef] [PubMed]
47. Wentrup, C. Carbenes and nitrenes: Recent developments in fundamental chemistry. *Angew. Chem. Int. Ed.* **2018**, *57*, 11508–11521. [CrossRef] [PubMed]
48. Wentrup, C. Flash vacuum pyrolysis of azides, triazoles, and tetrazoles. *Chem. Rev.* **2017**, *117*, 4562–4623. [CrossRef] [PubMed]
49. Wasylenko, W.A.; Kebede, N.; Showalter, B.M.; Matsunaga, N.; Miceli, A.P.; Liu, Y.; Ryzhkov, L.R.; Hadad, C.M.; Toscano, J.P. Generation of oxynitrenes and confirmation of their triplet ground states. *J. Am. Chem. Soc.* **2006**, *128*, 13142–13150. [CrossRef] [PubMed]
50. Sun, H.L.; Zhu, B.F.; Wu, Z.; Zeng, X.Q.; Beckers, H.; Jenks, W.S. Thermally persistent carbonyl nitrene: FC(O)N. *J. Org. Chem.* **2015**, *80*, 2006–2009. [CrossRef]
51. Li, H.M.; Wu, Z.; Li, D.Q.; Wan, H.B.; Xu, J.; Abe, M.; Zeng, X.Q. Direct observation of methoxycarbonylnitrene. *Chem. Commun.* **2017**, *53*, 4783–4786. [CrossRef]
52. Feng, R.J.; Lu, Y.; Deng, G.H.; Xu, J.; Wu, Z.; Li, H.M.; Liu, Q.; Kadowaki, N.; Abe, M.; Zeng, X.Q. Magnetically bistable nitrenes: Matrix isolation of furoylnitrenes in both singlet and triplet states and triplet 3-furylnitrene. *J. Am. Chem. Soc.* **2018**, *140*, 10–13. [CrossRef]
53. Yeh, P.-S.; Leu, G.-H.; Lee, Y.-P.; Chen, I.-C. Photodissociation of HNO_3 at 193 nm: Near-infrared emission of NO detected by time-resolved fourier transform spectroscopy. *J. Chem. Phys.* **1995**, *103*, 4879–4886. [CrossRef]
54. Tsao, M.-L.; Hadad, C.M.; Platz, M.S. A computational study of cyclopropylnitrene. *Tetrahedron Lett.* **2002**, *43*, 745–748. [CrossRef]
55. Becke, A.D. Density-functional thermochemistry. III. The role of exact exchange. *J. Chem. Phys.* **1993**, *98*, 5648–5652. [CrossRef]
56. Stratmann, R.E.; Scuseria, G.E.; Frisch, M.J. An efficient implementation of time-dependent density-functional theory for the calculation of excitation energies of large molecules. *J. Chem. Phys.* **1998**, *109*, 8218–8224. [CrossRef]
57. Foresman, J.B.; Head-Gordon, M.; Pople, J.A.; Frisch, M.J. Toward a systematic molecular orbital theory for excited states. *J. Phys. Chem.* **1992**, *96*, 135–149. [CrossRef]
58. Fukui, K. The path of chemical reactions – The IRC approach. *Acc. Chem. Res.* **1981**, *4*, 363–368. [CrossRef]

59. Hratchian, H.P.; Schlegel, H.B. Using hessian updating to increase the efficiency of a hessian based predictor-corrector reaction path following method. *J. Chem. Theory Comput.* **2005**, *1*, 61–69. [CrossRef] [PubMed]
60. Frisch, M.J.; Trucks, G.W.; Schlegel, H.B.; Scuseria, G.E.; Robb, M.A.; Cheeseman, J.R.; Scalmani, G.; Barone, V.; Mennucci, B.; Petersson, G.A.; et al. *Gaussian, 09*; Gaussian, Inc.: Wallingford, CT, USA, 2013.

Sample Availability: Samples of the compounds are available from the authors.